Mask Projection Microstereolithography of Novel Biocompatible Polymers

Philip Lambert[1*], Nicholas Chartrain[2*], Alison Schultz[3], Shelley Cooke[2], Timothy Long[3], Abby Whittington[2,4], Christopher Williams[1,2,5]

[1]Department of Mechanical Engineering, Virginia Tech
[2]Department of Materials Science & Engineering, Virginia Tech
[3]Department of Chemistry, Virginia Tech
[4]Department of Chemical Engineering, Virginia Tech
[5]Department of Engineering Education, Virginia Tech
*These authors contributed equally to this work

REVIEWED

Abstract

Mask Projection Microstereolithography (MPμSL) selectively cures entire layers of photopolymer to create three-dimensional parts with features on the micron scale. The resolution and scale of MPμSL are ideal for fabricating tissue engineering scaffolds with designed mesostructure. While MPμSL have excellent resolution, there are few biocompatible materials that are compatible with the vat photopolymerization processes. A novel diacrylate functionalized Pluronic L-31 block-copolymer and poly(propylene glycol diacrylate) were synthesized and processed with MPμSL. The resulting structures were analyzed for biocompatibility, as well as accuracy and mechanical strength to assess feasibility for use in tissue engineering scaffold fabrication. Preliminary fabricated scaffold geometries are presented to validate experimental results.

1. Introduction

1.1. The Need for Tissue Engineering Scaffolds

The goal of Regenerative Medicine is to repair or replace damaged or diseased tissues to reestablish normal functionality. Tissue Engineering uses cells, materials, and physical or chemical stimuli to create Tissue Engineering constructs that can be used as tissue replacements [1, 2]. Often, stem cells are chosen because they have the ability to differentiate into multiple cell types. By differentiating these stem cells into a variety of cell types, the Tissue Engineering construct possesses greater functionality than those engineered with a single differentiated cell type [2].

The role of a Tissue Engineering scaffold is to provide cells with both mechanical support and an environment that has enough porosity to allow for diffusion of essential nutrients [3, 4]. Performance of a tissue engineering scaffold has been shown to be dependent on the structure, specifically the porosity and pore size, of the matrix. Highly porous support structures are favorable for mass transport, delivering cell mass for tissue regeneration [5]. Furthermore, high porosity is desirable for diffusion of nutrients and waste products to and from the tissue growth, as well as for vascularization, which are requirements for successful cell growth. While a large surface area favors cell attachment, the surface area/volume ratio of a porous material is dependent on density and diameter of pores. Furthermore, the diameter of the cells dictates the minimum pore size. When defining porosity and pore size, considerations must be made such that scaffolds retain good mechanical properties while also being permeable and porous for the

974

transport of cells and nutrients [5, 6]. Managing the tradeoff between porosity and mechanical strength poses a significant challenge for the field of Tissue Engineering.

Incorporating vascularization into Tissue Engineering scaffolds has often been cited as the most significant barrier in the field [7]. Insufficient vascularization, the lack of vessels that allow for nutrient diffusion and mass transport to cells, leads to apoptosis. Artificial skin constructs, which have shown success in clinical settings, have little need for built-in vascularization because they are thin enough to allow for adequate diffusion through them [8]. However, a vascular network is essential for tissues thicker than a few hundred microns. A majority of the organs which are in scarce supply for transplant, such as the kidney, liver, pancreas, and heart, are thick solid tissues. To reconstruct these complex tissues, it is necessary to create Tissue Engineering scaffolds with adequate vascularization.

1.2. Additive Manufacturing of Tissue Engineering Scaffolds

Conventional fabrication techniques including particulate leeching, gas foaming, and electrospinning have often been used to create tissue engineering scaffolds [1, 9]. Unfortunately, these techniques have a number of shortcomings that make them less than idea for tissue engineering scaffold fabrication. Most notably, these techniques do not control the precise placement of material in the scaffold. While particulate leeching is able to control pore size and electrospinning produces fibers of a known diameter, these techniques cannot control tortuosity and pore size, placement and distribution all at the same time [10]. The resulting scaffolds are not optimized for cell growth and mechanical strength. Figure 1 (left) shows a poorly optimized scaffold made by gas foaming that has high surface area and porosity, but low mechanical strength and pore interconnectivity [11]. This lack of pore interconnectivity results in a poorly vascularized scaffold that cells will have trouble permeating through. Figure 1 (right) shows a scaffold that has small feature sizes and good pore interconnectivity but a random distribution of pores throughout the scaffold [12].
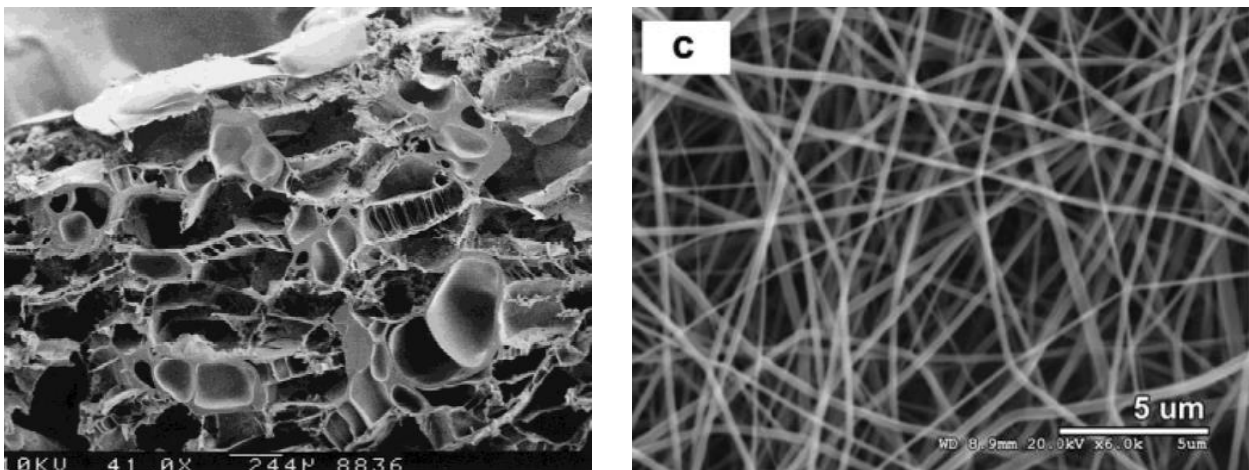

Figure 1: A scaffold fabricated via gas foaming (left) [11] and one made via electrospinning (right) [12]

Additive Manufacturing (AM) technologies allow for the selective placement of material and allow for the fabrication of scaffolds with designed geometries that can be optimized for Tissue Engineering. These techniques use an additive, layer-by-layer manufacturing process, where the

geometry of each layer can be designed and controlled. Stacking these layers in a consecutive fashion enables the design of complex 3D parts. The advantage of AM in Tissue Engineering is the ability to control both microstructure, which enables the creation of vascularization, as well as macrostructure. Several AM processes have been considered for scaffold fabrication, including selective laser sintering, extrusion, binder jetting, and Stereolithography [4, 13-15].

It is important to be able to fabricate scaffolds with feature that are comparable in size to the cells that will be seeded onto them (on the order of 10 μm) [16]. Scaffolds with feature sizes that do not extend down into this range will not allow for as much surface area onto which cells can attach nor would they provide the extensive vascularization that is essential for an optimized tissue engineering scaffold. Fused Deposition Modeling (FDM) is often considered as a candidate for creating scaffolds because it can create relatively large objects rapidly [15]. It is also an inexpensive process and it is simple to lay down filament in offset patterns to make scaffold like structures. However, as can be seen in Figure 2, the smallest pore sizes that can be achieved with FDM processes are often 500 μm or greater in diameter and the geometries are typically limited to "log-cabin" lay-ups of overlapping extrudate roads that feature periodic cell morphologies [14]. Scaffolds made via binder jetting and selective laser sintering present similar drawbacks due to the relatively large powder particles [17-19]. Systems that extrude cells directly onto the build platform have become quite popular recently. These systems, such as the 3D Bioplotter produced by EnvisionTEC and custom machines of similar design have the ability to place differentiated cells precisely where they are desired [20, 21]. However, the tissue engineering constructs that these systems fabricate are hydrogels or other materials which have little mechanical strength. In addition, cells need to be kept viable during the printing processes. The cells are generally extruded in relatively large numbers instead of one by one, which lessens the control that one has over the placement of material in the construct. Given the goal of fabricating designed scaffolds with vascularization pathways on the micron scale, the authors chose Microstereolithography as a manufacturing platform due to its excellent resolution despite the disadvantage that it does not directly incorporate cells into the fabrication process.
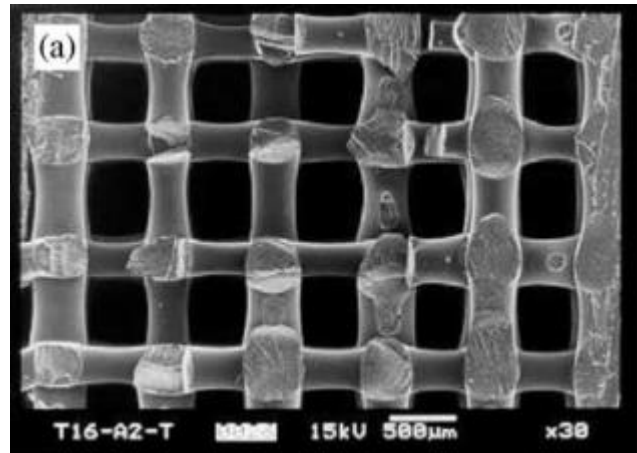

Figure 2: A scaffold fabricated via FDM[14]

1.3. Mask Projection Microstereolithography (MPμSL)

Mask Projection Microstereolithography is a relatively new Additive Manufacturing technique capable of fabricating complex three-dimensional structures with micron-sized features [18]. When a photopolymer is exposed to light of sufficient energy and intensity, a crosslinking process is initiated that results in the solidification of a polymeric network. Microstereolithography systems use a dynamic mask to pattern light as opposed to a scanning laser used in Stereolithography systems. Mask Projection systems use digital light processing (DLP) technology to create a dynamic mask that can be projected onto the surface of the

976

prepolymer all at once. Ultraviolet light is created by a lamp, LED, or laser and is conditioned with a series of optics that can include collimating lenses, wavelength filters, and homogenizing rods. The light is projected onto a digital micromirror device (DMD) that is made up of hundreds of small mirrors that pattern the light and selectively project it onto the surface of the prepolymer. A number of research groups have created Microstereolithography systems and used them to create tissue engineering scaffolds [4, 16, 22-27].

1.4. Biocompatible Photopolymers
    Unfortunately, the majority of photopolymers do not exhibit strong biocompatibility[4]. Poly (propylene fumarate) (PPF) is the most widely used biocompatible and bioresorbable photopolymer in Stereolithography with tissue engineering scaffold applications [23, 27-32]. Several researchers have used other biocompatible polymers in an attempt to create tissue engineering scaffolds with a wider range of properties [4, 33]. However, the number and diversity of photopolymers that have been shown to be biocompatible is quite small. To further the use of this high-resolution AM process for fabricating tissue engineering scaffolds, it is crucial to identify and develop novel biocompatible photopolymers with a variety of mechanical and chemical properties that can be used in tissue engineering scaffolds.

    To address this gap in the research, two photopolymers were investigated: Pluronic L-31 diacrylate and poly(propylene glycol diacrylate) (PPGDA). Pluronic L-31 is a novel block copolymer not before used in MPµSL that contains blocks of poly(ethylene glycol) (PEG) and poly(propylene glycol) (PPG), and was chosen as this family of materials has been reported to be biocompatible [34]. In addition, Pluronic L-31 is a commercially available diol available in a range of molecular weights that undergoes a facile functionalization reaction allowing it to be UV cureable telechelic diacrylate. The pluronic family of materials consists of block copolymers made up of PPG and PEG blocks of various lengths and arrangement. These block copolymers have higher order structures than polymers made up of just a single monomer. In addition, differences in solubility of the PPG and PEG blocks may impart additional nanoscale structure for optimizing cell adhesion. Applying Pluronics with variable block segment lengths and arrangements will provide control over the nanoscale morphology of the material.

    Although readily available and considered to have acceptable biocompatibility, PPGDA has not been processed via MPµSL. The effects of the poly(ethylene glycol) endgroups on the Pluronic L-31 will be investigated by comparing the results obtained from PPGDA and Pluronic L-31.

    In Section 2, the MPµSL processs – both the apparatus and the process model – is explained. Section 3, describes the materials and experimental methods used to answer following specific research questions:
    - What are the process parameters that will allow for PPGDA and Pluronic L-31 to be fabricated?
    - What are the minimum feature sizes and accuracies that the MPµSL system can achieve with these materials?
    - What are the mechanical properties of these materials and how do they compare to actual tissue?

-   Do PPGDA and Pluronic L-31 have adequate biocompatibility to be used as materials in tissue engineering scaffolds?

Section 4, presents and discusses the results obtained from implementing these methods. Finally, in Section 5, general conclusions and future research opportunities are explored.

2. **Mask Projection Microstereolithography**

2.1. MPµSL Machine

The MPµSL machine shown in Figure 3 was developed at Virginia Tech and consists of a UV light source, conditioning optics, a mirror, a dynamic mask connected to a computer, imaging optics, and a prepolymer container with a stage mounted on a linear actuator [35]. A LightningCure LC-L1V3 UV LED system by Hamamatsu was chosen as a source of ultraviolet light. The conditioning optics (Edmund Optics) ensure that the entire dynamic mask is illuminated by UV light while the imaging optics focus the patterned light onto the prepolymer surface and reduce the image dimensions by a factor of two. The dynamic mask, a FlexLight X1 DLP Development System (Keynote Photonics) consists of a DLP 0.95 1080p DMD from Texas Instruments and a developer board. The DMD is a 1920 x 1080 array of aluminum micromirrors that measures 0.95-inch along the diagonal. Each square micromirror has a side length of 10.8 µm. The imaging optics reduce the image dimensions by a factor of 2 so the effective projection area of each micromirror on the surface of the photopolymer surface is 5.4 µm x 5.4 µm. Due to the optics of the system, the maximum part size in the XY plane is 6mm by 8mm. The Z direction is currently limited to 36mm. A linear actuator (Zaber NA11B60) was used to control the movement of a custom stage made by Fused Deposition Modeling (FDM).
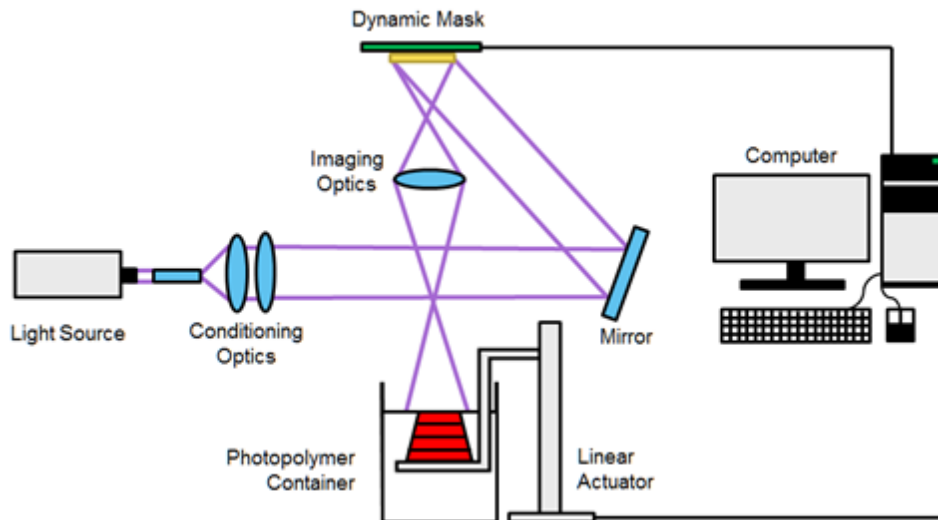

Figure 3: Schematic of the Mask Projecting Microstereolithography machine

2.2 Fabrication Process

Like most Additive Manufacturing processes, Microstereolithography fabricates parts from a computer aided design (CAD) file [18]. The Microstereolithography Fabrication process begins

first by slicing a three-dimensional CAD model into individual images that can be projected onto the prepolymer surface. One can use an Additive Manufacturing software environment, such as NetFabb to create slices (saved as bitmap images) of a desired thickness (25 μm was used).

A LabView program was used to control the projection of these images by the DMD and the movement of the stage. The prepolymer container was filled and the stage lowered until it was just submerged. The LabView program then turned individual mirrors "on" or "off" to represent the first image. The UV light passed from the LED lamp through the conditioning optics and mirror to the DMD. This resulted in the image being projected from the DMD onto the thin layer of prepolymer directly above the stage. The image was projected for a certain amount of time based upon the working curve of the material being used (generally between one and five seconds). After this set time, the DMD mirrors are turned "off" so that no light is projected into the prepolymer container and the stage is lowered into the container. The stage was completely submerged and then returned to one layer thickness below the surface. The LabView software loads the next layer's image and the process was repeated until the part was completely fabricated.

After the part has been fabricated, the stage was removed and the part separated from the stage with a blade. The part was washed with a few drops of isopropyl alcohol (IPA) to remove any uncured prepolymer. The part can then be post-cured by placing it in the path of the UV lamp. This helps to ensure that the polymer was fully crosslinked.

2.3 The Working Curve

To successfully process photopolymers via Stereolithography, one must first determine its two characteristic material properties: critical exposure (*Ec*) and depth of penetration (*Dp*). The Working Curve, first presented by Jacobs in 1992 provides a means of determining these two parameters [18, 36]. The expression is based on the Beer-Lambert law of absorption and is defined as:

$$C_d = D_p \ln(E/E_C)$$

The Working Curve relates the exposure of light provided at the prepolymer surface (*E*) and the depth to which the prepolymer is crosslinked into a polymer (cure depth, *Cd*). The minimum exposure required to begin polymer crosslinking is the critical exposure (*Ec*).

It is essential to determine the Working Curve of a polymer that is to be fabricated so that the prepolymer surface can be exposed to the necessary amount of UV energy for polymer curing. To determine the working curve, one provides a series of varied exposures to the resin surface and measures the thickness of the resulting thin film. The thickness at each exposure is plotted on a semi-log plot; the working curve typically shows a linear relationship between the cure depth and the natural log of exposure. The critical exposure is located at the resultant curve's x-intercept and depth of penetration is determined by analyzing the slope of the curve. Additional details are provided in Section 3.2.1.

3. **Materials and Methods**

To fabricate PPGDA and Pluronic L-31 via Microstereolithography and characterize these polymers, a variety experimental methods and materials were utilized. The methods were used

to determine the processing parameters and mechanical properties of the polymers, their biocompatibility, and the minimum feature size and accuracy achievable with the MPµSL system.

3.1 Materials

PPGDA, a polyfunctional acrylic monomer, was acquired from Sigma Aldrich (CAS 52496-08-9). Pluronic L-31 was acquired from Sigma Aldrich (CAS 9003-11-6). Biological materials including Dulbecco's phosphate buffered saline (DPBS), media (10% fetal bovine serum and 1% Pen/Strep to media composition), trypsin, trypan blue, fibronectin, and calcein AM and eithidium homodimer dyes were purchased from Invitrogen (Carlsbad, CA). The MC3T3-E1 cell culture was obtained from the American Type Culture Collection (ATCC). The CellTiter 96 AQueous One Solution Cell Proliferation MTS Assay (3-(4,5-dimethylthiazol-2-yl)-5-(3-carboxymethoxyphenyl)-2-(4-sulfophenyl)-2H-tetrazolium) was obtained from Promega (Madison, WI).

3.1.1 *Poly (Propylene Glycol) Diacrylate*

The PPGDA had an average molecular weight (Mn) of 800, and contains 100 ppm of both BHT (butylated hydroxytoluene) and MEHQ (mono methyl ether of hydroquinone) which act as photoinhibitors and prevent the polymerization of the PPGDA during normal handling. PPGDA contains reactive diacrylate end groups and thus required no functionalization to allow for UV curing.

3.1.2 *Pluronic L-31 Functionalization*

Pluronic L-31 is a difunctional block copolymer with chemical formula poly(ethylene glycol)-block-poly(propylene glycol)-block-poly(ethylene glycol). The Pluronic L-31 used in this study consisted of a central block of 17 PPG monomers terminated on either end by one PEG monomer. The Pluronic L-31 exhibits both hydrophilic (derived from the PEG monomers) and hydrophobic properties (derived from the PPG monomers). The Pluronic L-31 prepolymer was functionalized with reactive diacrylate end groups, making it compatible with the photo-crosslinking process. The functionalized oligomer is shown in Figure 4.
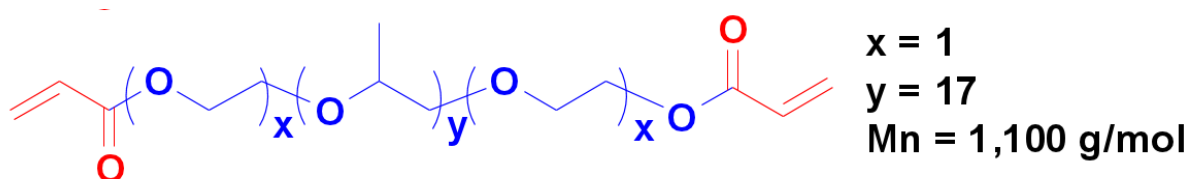

Figure 4: Pluronic L-31 functionalized with reactive diacrylate end groups shown in red

3.1.3 *Prepolymer Preparation*

Photopolymers on their own will not crosslink in the presence of UV light [18]. They require the addition of small amounts of photoinitiator to catalyze the reaction. The photoinitiator absorbs the UV light and creates a reactive intermediary that begins the crosslinking process [26]. For the chemistries described in this research, crosslinking occurs via the free-radical polymerization process. Two weight percent of the photoinitiator (2,2-dimethoxy-2-phenylacetophenone, Sigma Aldrich CAS 24650-42-8) (DMPA) was dissolved in a small amount of acetone and added to both the PPGDA and functionalized Pluronic L-31.

Photoinitiator concentrations were kept as low as possible while still permitting for the polymer to be UV cured as the photoinitiator is known to be cytotoxic.

3.2 Experimental Methods

3.2.1 Determination of the Working Curve

Before the fabrication of parts, the Working Curve of each polymer was calculated to determine the processing parameters of each material [36]. To accomplish this, the prepolymer surface was illuminated fully by the DMD with a known exposure (4.9 mW/cm^2) and duration to create a thin film [18]. These films were then measured with a micrometer to determine their cured thickness. Several films (n=4) were created for four different exposure values. The film thicknesses and their associated exposures were entered into a MatLab program that plots the exposure versus the cure depth. The critical exposure and depth of penetration parameters were extracted from the resulting graph. With these parameters, the exposure required to fabricate a film of desired thickness can be calculated.

3.2.2 Film and Benchmark Part Fabrication

Films of PPGDA and Pluronic L-31 were created to test cell viability on each material. Films provide an easy surface on which to seed cells and can be easily fabricated. The films were fabricated by placing 0.25 mL of either PPGDA or Pluronic L-31 with 2 wt% photoinitiator into 24 well plates and passed under a high power UV light source for 6 seconds to crosslink the prepolymer. The films were passed under the light source eight times to ensure that the polymer was fully crosslinked. Each well was rinsed with IPA to remove any uncured prepolymer from the surface of the film.

A benchmark part was designed to determine the XY minimum feature size, the XY accuracy, the Z minimum feature size and the Z accuracy of the machine and polymer. The part was designed to be sliced and fabricated with 25 micron layers. The cylindrical extrusions on the top plane of the part incrementally reduce in diameter from 200 microns to 5 microns along both the X and Y axes. These cylinders are used to measure the minimum feature size achievable in the XY plane. The cross-shaped extrusions on the top plane of the part all have the same dimensions and are located equidistant from one another. By measuring the relative distances of the cross-features, the accuracy of the XY plane can be determined. The third feature on this part is the cross beam on the four lateral faces. Measuring the thickness of the cross beams allows for the determination of the Z-dimension accuracy. The final set of features are the extrusions on the XZ and YZ faces. These extrusions range in Z height thickness from 200 microns to 25 microns. Measuring the thickness of the smallest structure, the Z accuracy and minimum Z axis feature size can be determined.

To construct the test parts shown in the CAD model in Figure 5, the model was first sliced into 25 μm layers in NetFabb. These images were projected onto the material systems at a light intensity of 4.9 mW/cm^2 for an amount of time to achieve a 25 μm cure depth as determined by the working curve. The remainder of the fabrication was carried out according to the procedure described in Section 2.2. After the parts were fabricated, they were left to dry, rinsed with IPA, and measured using a DinoLight Digital microscope.
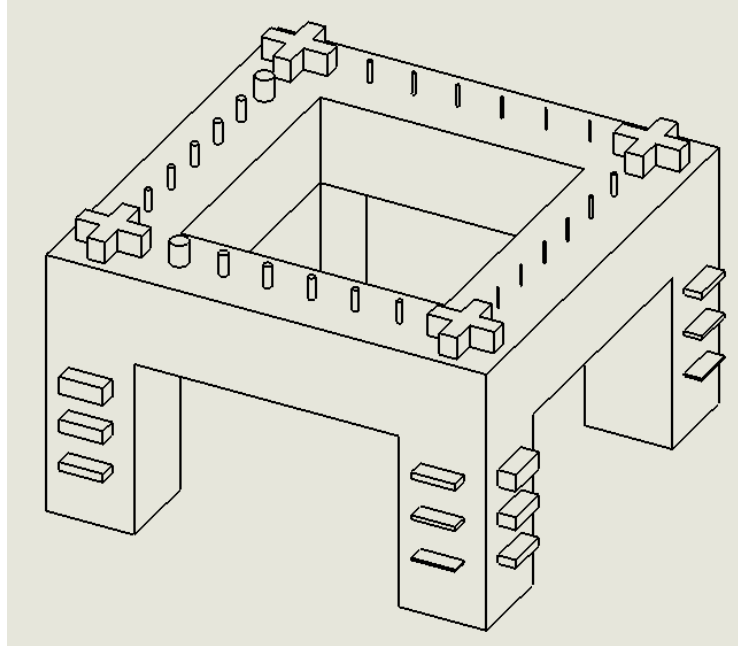
Figure 5: Isometric image of the benchmark characterization part

3.2.3 *Mechanical Testing*

Mechanical testing was conducted in order to compare the mechanical properties of the polymers being used to those of actual tissues. Clearly, the polymers must be strong enough to provide a supporting structure on which the cells can grow but should not be significantly stronger than the tissue that they intend to replace [5]. There will always be some mismatch between the stiffness and hardness of tissues and the biomaterials intended to replace them, but reducing this disparity is critical to creating viable tissue engineering scaffolds.

Thin films of PPGDA and Pluronic L-31 were cured in teflon petri dishes using a high power broadband UV light source to impart 222 mJ/cm^2 of exposure. Each well was rinsed with IPA to remove any uncured prepolymer from the surface of the film. The films were then trimmed into rectangles approximately 5mm wide and 20mm long with a razor blade. The samples were tested using an Intron 5500R and Bluehill 2 Instron Software package at a strain rate of 5mm/min.

3.3 Cell Culture

A cell study was conducted to determine the biocompatibility of the PPGDA and Pluronic L-31. Materials used in tissue engineering scaffolds cannot be cytotoxic or cells will be unable to grow on them. In particular, the photoinitiator DMPA is known to be toxic. To reduce the toxicity of the cured materials, the amount of DMPA added to the prepolymer was kept as low as possible while still allowing for polymerization to occur (2 wt% DMPA). MC3T3-E1 mouse preosteoblasts were seeded onto films fabricated in the bottom of polystyrene cell culture plates. Cell viability was quantified using an MTS assay after culturing the cells for 1, 4, and 7 days.

3.3.1 *Cell Seeding and Cytotoxicity*

Films were sterilized by spraying them with 70% ethanol and exposing them to UV light for 1 hour. The UV light intensity used to sterilize the films was significantly less than that of the

Microstereolithography system so it was not expected to have any impact on the polymer's mechanical properties. Cell media was placed on PPGDA and Pluronic L-31 films for 30 minutes in preparation for cell seeding. Half of the films also received fibronectin (1mg/mL of media) to promote cell adhesion to the films. MC3T3-E1 mouse preosteoblasts were trypsinized, counted, and resuspended in fresh media. The cells were seeded at a density of 10^4 cells/cm^2 of surface area of the film. This corresponded to 19,000 cells being placed on each film. The same quantity of cell suspension was also added to tissue culture treated polystyrene well plates as a control. The cells were given one hour to attach to the films and then the media was removed. The wells were then filled with fresh media containing 10% fetal bovine serum (FBS) and 1% Penicillin Streptomyacin.

3.3.2 Cell Viability

Cell survival and proliferation for films and tubes was measured on days 1, 4, and 7 after seeding. Cells grown for 1 and 4 days did not receive fresh media while those grown for 7 days received fresh media on the fourth day. An MTS assay, was used to quantify the number of cells on the films and tubes. To create a control curve, 100, 1,000, 10,000, 100,000, 500,000 cells were suspended in 100 µl of media in wells. 20 µl of the MTS assay was added to each and allowed to incubate for four hours at 37°C. The 120 µl was then transferred into a 96 well plate and the absorbance was measured at 490 nm. To quantify the number of cells on the films and scaffolds, the media was removed from the respective wells and 100 µl of fresh media was added. 20 µl of the MTS assay was added and the cells were incubated for 4 hours at 37°C. The media and MTS assay were transferred to a 96 well plate and their absorbance was measured. The number of cells on each scaffold and film was determined by comparing the measured absorbance to a fit of the control curve.

4. **Results and Discussion**

4.1 Determination of Working Curve

The critical exposure of the PPGDA with 2 wt% photoinitiator was found to be 6.05 mJ/cm^2 and the depth of penetration was 398 µm. Characterization of the Pluronic L-31 with 2 wt% photoinitiator found the critical exposure to be 17.2 mJ/cm^2 and the depth of penetration to be 289 µm. These parameters were used when fabricating the benchmark parts.
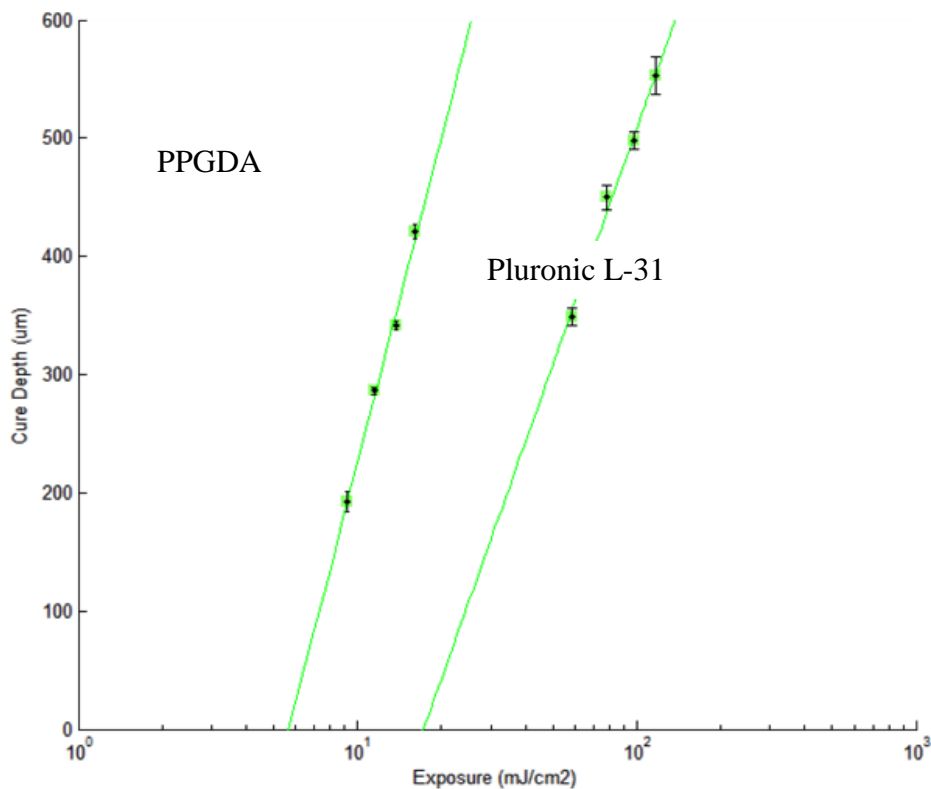
Figure 6: Working Curves for PPGDA and Pluronic L-31 both with 2 wt% photoinitiator

4.2 Machine Capabilities

The benchmark part described in Section 3.2.2 was fabricated three times and its features were measured to determine accuracy and minimum achievable feature size. The results obtained were dependent not only on the accuracy and precision of the system, but also on the material in use. This difference could be attributed to the differences in nanostructure between the Pluronic L-31 and the PPGDA. The coblock structure of the Pluronic L-31 might allow it to collapse on itself. Further investigation will be necessary to understand why different polymers yield minimum feature sizes that are so different. The XY axis minimum feature size was determined by measuring the diameter of the smallest cylinder that was successfully fabricated in this plane. The smallest fabricated cylinder of the PPGDA sample averaged 212 μm in diameter while the Pluronic L-31 benchmark parts contained significantly smaller cylinders of just 57 μm in diameter.
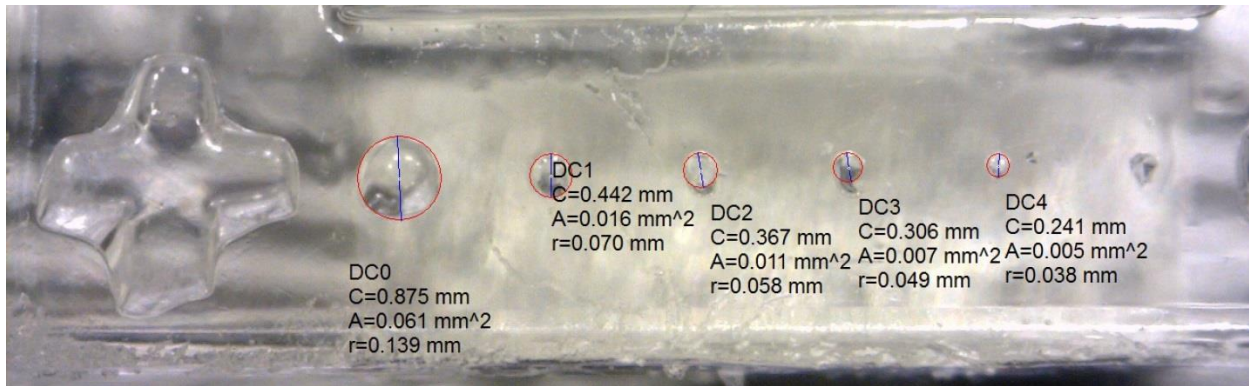
Figure 7: X axis measurements for minimum feature size analysis on a benchmark part fabricated with PPGDA

Sixteen key measurements were made on each sample to determine the dimensional accuracy of the system in the XY plane. The average error in the XY plane was found to be 2.5% for PPGDA and 6% for Pluronic L-31.

Table 1: Summary of Machine Capabilities using both PPGDA and Pluronic L-31

	PPGDA	Pluronic L-31
Minimum Feature Size in XY Plane	212 μm	57 μm
Error in XY Plane	2.5%	6%
Error in Z Axis	119%	83%

The Z accuracy of the system with both the PPGDA and Pluronic L-31 was extremely poor due to a print-through effect. In fact, the only meaningful quantitative value that could be determined was the thickness of the cross beam. As the cross beam in most parts generated an arc-like shape, the measurement was made at the center of the beam for consistency.   These measurements showed a 119% error in observed thickness when compared to designed thickness for the PPGDA and an 83% error for the Pluronic L-31. The lack of lateral definition was somewhat expected due to the high depths of penetration (Dp) of the PPGDA and Pluronic L-31 with 2wt% initiator.

Despite the error observed in the Z axis accuracy, some parts were fabricated that showed good resemblance when compared to their intended designs. The 4mm x 4mm x 8mm scaffold shown in Figure 8 (left) was designed to resemble a possible tissue engineering scaffold. A Micro Computed Tomography (Micro CT) scan of the fabricated scaffolds are shown in Figure 8. Arching can be seen below the horizontal crossbeams suggesting error in Z dimensional accuracy, however the parts maintain similarity to the design.
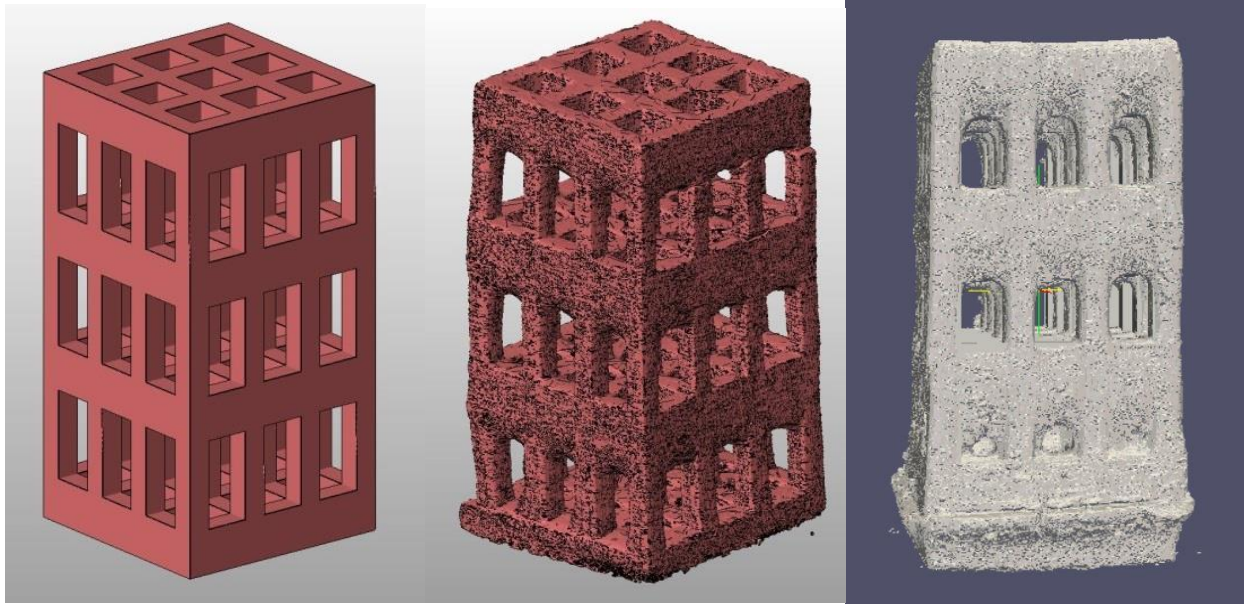
Figure 8: CAD model of designed scaffold (left). Micro-CT scan model of the fabricated PPGDA scaffold (middle) and Pluronic L-31 (right)

The vertical build rate is highly dependent on the prepolymer properties such as critical exposure and viscosity. With higher critical exposure, a prepolymer takes longer to reach the gel point, and extends the time per layer. Similarly, the viscosity of the prepolymer contributes to the refresh duration required after the dipping recoat process. Higher viscosity prepolymers take longer to settle, extending the time per layer, and thus the vertical build rate. The vertical build rates for PPGDA and Pluronic L-31 with parts sliced in 25 μm layers were found to be approximately 360 layers per hour and 325 layers per hour respectively. A 5mm tall part with 25 μm layers made of PPGDA would take approximately half an hour to complete.

4.3 <u>Mechanical Testing</u>
The mechanical strengths of both the PPGDA and Pluronic L-31 were found to be physiologically relevant. The Young's Modulus and largest observed strengths of both materials were slightly higher than that of aortic tissue, while still significantly less than that of skin. The largest strains observed in both materials were somewhat inferior to those of the human tissues. While both polymers had Young's Moduli that were similar to those of human tissue, the PPGDA was significantly stiffer than the Pluronic L-31. The PEG endgroups of the Pluronic L-31 may have adversely impacted its stiffness while imparting additional ductility. Additionally, it is possible that the block copolymer structure of the Pluronic L-31 may have allowed the material to expand and contract elastically.

Table 2: Summary of the mechanical testing results of PPGDA, Pluronic L-31 and literature values for skin and aorta

	PPGDA	Pluronic L-31	Skin[37, 38]	Aorta[39]
Young's Modulus (MPa)	9.64 ± 1.48	3.41 ± 0.27	50-100	2-3.2
Ultimate Tensile Strength (MPa)	1.04 ± 0.30	0.74 ± 0.12	1-20	0.3-0.8
Ultimate Tensile Strain (%)	13.14 ± 3.77	26.9 ± 2.66	30-70	50-100

4.4 Cell Viability

The cell viability assay conducted show that both the PPGDA and Pluronic L-31 are not cytotoxic. Although extensive cellular growth did not occur after 7 days, the continued presence of the cells on the material is meaningful enough to warrant additional investigation into these materials. In addition, the PPGDA and the PPG blocks of the Pluronic L-31 are highly hydrophobic and thus significantly fewer cells should be expected on these materials when compared to the hydrophilic polystyrene. Furthermore, these results are consistent with the hydrophillic PEG endgroups of the Pluronic L-31 that make it somewhat more biocompatible than the PPGDA.
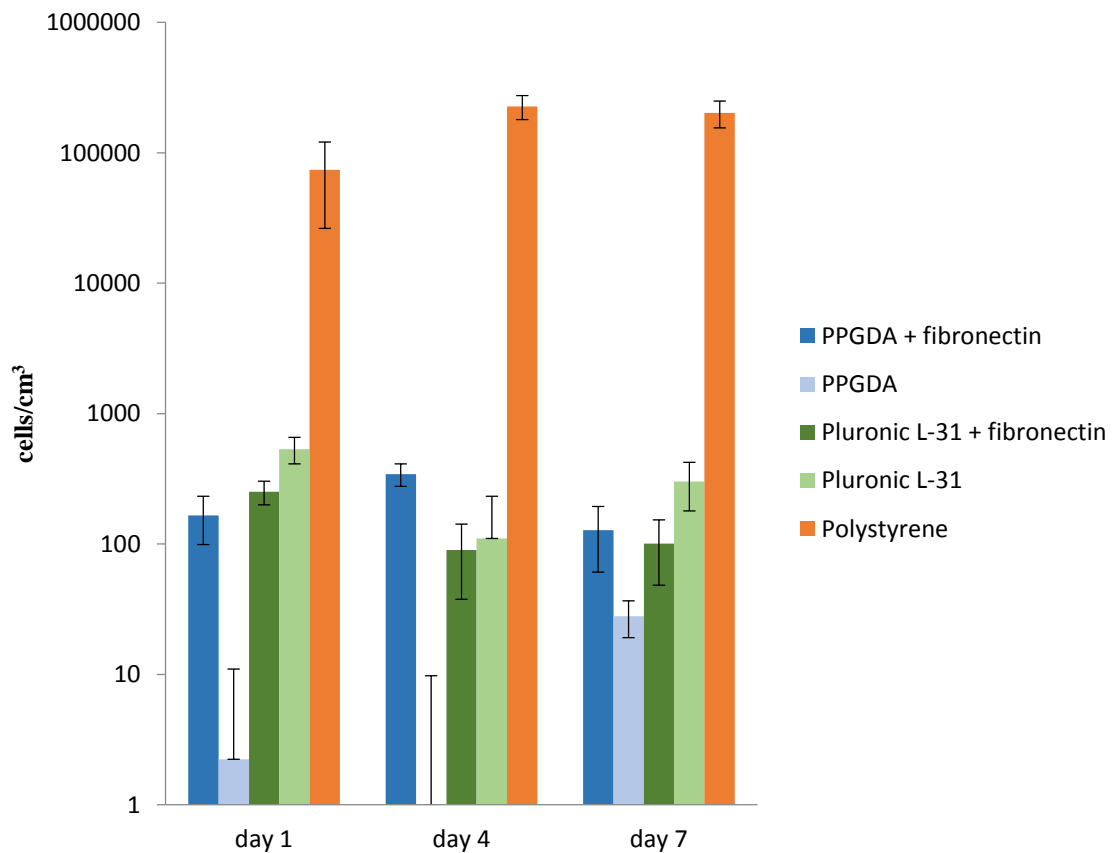

Figure 9: MTS Cell Assay results after 1, 4, and 7 days of cell culture on UV cured films

5. Conclusions and Future Work

This research has demonstrated the processability of the novel photopolymers PPGDA and Pluronic L-31 via MPµSL to fabricate parts with features on the micron scale. These materials were found to have mechanical properties similar to those of human tissue and a seven day cell assay found that the polymers were not cytotoxic. In addition, it was shown that the PEG endgroups on the Pluronic L-31 had a discernable effect on not only the mechanical and biocompatibility properties of the material but also on the minimum feature size that could be achieved.

These results warrant further investigation into the application of these materials into tissue engineering scaffolds. Future work will focus on seeding cells onto three dimensional scaffolds and observing their growth, migration, and differentiation. In addition, the effect of the Pluronic L-31's block copolymer structure on both the nanoscale and microscale structure of objects processed by MPµSL will be investigated. Finally, chemical cues (e.g. growth hormones, collagen) will be incorporated into the tissue engineering scaffolds to improve biocompatibility and cell division.

References

1. Atala, A., *Engineering organs.* Current opinion in biotechnology, 2009. **20**(5): p. 575-92.
2. Atala, A., *Regenerative medicine strategies.* Journal of pediatric surgery, 2012. **47**(1): p. 17-28.
3. Leong, B.P.C.a.K.W., *Scaffolding in tissue engineering: general approaches and tissue-specific considerations.* Eur. Spine J., 2008. **17**(4): p. 467-79.
4. Melchels, F.P.W., J. Feijen, and D.W. Grijpma, *A review on stereolithography and its applications in biomedical engineering.* Biomaterials, 2010. **31**(24): p. 6121-6130.
5. Hollister, S.J., *Porous scaffold design for tissue engineering.* Nature Materials, 2005. **4**(July).
6. Yang, S., et al., *The Design of Scaffolds for Use in Tissue Engineering Part II. Rapid Prototyping Techniques.* Tissue Engineering, 2002. **8**(1): p. 1-12.
7. Novosel, E.C., C. Kleinhans, and P.J. Kluger, *Vascularization is the key challenge in tissue engineering.* Advanced drug delivery reviews, 2011. **63**(4-5): p. 300-11.
8. Phelps, E.a. and A.J. García, *Engineering more than a cell: vascularization strategies in tissue engineering.* Current opinion in biotechnology, 2010. **21**(5): p. 704-9.
9. Gauvin, R., et al., *Microfabrication of complex porous tissue engineering scaffolds using 3D projection stereolithography.* Biomaterials, 2012. **33**(15): p. 3824-3834.
10. Kundu, J., et al., *Biomaterials for Biofabrication of 3D Tissue Scaffolds*, G. Forgacs and W. Sun, Editors. 2013, Elsevier Inc. p. 23-46.
11. Harris, L.D., B.S. Kim, and D.J. Mooney, *Open pore biodegradable matrices formed with gas foaming.* Journal of biomedical materials research, 1998. **42**(3): p. 396-402.
12. Lee, S.J., et al., *Development of a composite vascular scaffolding system that withstands physiological vascular conditions.* Biomaterials, 2008. **29**(19): p. 2891-8.
13. Melchels, F.P.W., et al., *Additive manufacturing of tissues and organs.* Progress in Polymer Science, 2012. **37**(8): p. 1079-1104.

14. Zein, I., Hutmacher, D. W., Tan, K. C., & Teoh, S. H., *Fused deposition modeling of novel scaffold architectures for tissue engineering applications. Biomaterials.* Biomaterials, 2002. **23**(4): p. 1169-1185.

15. Chhaya, M.P., et al., *Breast Reconstruction Using Biofabrication-Based Tissue Engineering Strategies*, G. Forgacs and W. Sun, Editors. 2013, Elsevier Inc. p. 183-216.

16. Choi, J.-W., et al., *Fabrication of 3D biocompatible/biodegradable micro-scaffolds using dynamic mask projection microstereolithography.* Journal of Materials Processing Technology, 2009. **209**(15-16): p. 5494-5503.

17. Liu, C., Z. Xia, and J.T. Czernuszka, *Design and Development of Three-Dimensional Scaffolds for Tissue Engineering.* Chemical Engineering Research and Design, 2007. **85**(7): p. 1051-1064.

18. Gibson, I., D. Rosen, and B. Stucker, *Additive Manufacturing Technologies Rapid Prototyping to Direct Digital Manufacturing*. 2010.

19. Hutmacher, D.W., *Scaffold-based Tissue Engineering – Design and Fabrication of Matrices Using Solid Freeform Fabrication Techniques*, I. Gibson, Editor. 2006.

20. Ozbolat, I.T., H. Chen, and Y. Yu, *Development of 'Multi-arm Bioprinter' for hybrid biofabrication of tissue engineering constructs.* Robotics and Computer-Integrated Manufacturing, 2014. **30**(3): p. 295-304.

21. Xu, T., et al., *Regenerative Medicine Applications in Organ Transplantation*. 2014.

22. Lee, S.-J., et al., *Application of microstereolithography in the development of three-dimensional cartilage regeneration scaffolds.* Biomedical microdevices, 2008. **10**(2): p. 233-41.

23. Woo, J., et al., *Biomaterials Bone regeneration using a microstereolithography-produced customized poly (propylene fumarate)/diethyl fumarate photopolymer 3D scaffold incorporating BMP-2 loaded PLGA microspheres.* Biomaterials, 2011. **32**(3): p. 744-752.

24. Leigh, S.J., et al., *Fabrication of 3 - Dimensional Cellular Constructs via Microstereolithography Using a Simple, Three-Component, Poly(Ethylene Glycol) Acrylate-Based System.* Biomacromolecules, 2013. **14**: p. 186-192.

25. Bertsch, A., et al. *Microstereolithography: a Review*.

26. Cho, D.-W. and H.-W. Kang, *Microstereolithography-Based Computer-Aided Manufacturing for Tissue Engineering*, M.A.K. Liebschner, Editor. 2012. p. 341-356.

27. Lee, J.W., et al., *Scaffold Fabrication with Biodegradable Poly(propylene fumarate) Using Microstereolithography.* Key Engineering Materials, 2007. **342-343**: p. 141-144.

28. Hwal, J., et al., *Evaluation of cell proliferation and differentiation on a poly (propylene fumarate) 3D scaffold treated with functional peptides.* Journal of Materials Science, 2011. **46**: p. 5282-5287.

29. Lee, J.W., et al., *3D scaffold fabrication with PPF/DEF using micro-stereolithography.* Microelectronic Engineering, 2007. **84**(5-8): p. 1702-1705.

30. Xuan, P., et al., *Development of 3D PPF / DEF scaffolds using micro-stereolithography and surface modification.* Journal of materials science. Materials in medicine, 2009. **20**: p. 271-279.

31. Lee, J.W., et al., *Development of nano- and microscale composite 3D scaffolds using PPF/DEF-HA and micro-stereolithography.* Microelectronic Engineering, 2009. **86**(4-6): p. 1465-1467.

32. Cho, D.-W., et al., *Estimation of cell proliferation by various peptide coating at the PPF/DEF 3D scaffold.* Microelectronic Engineering, 2009. **86**(4-6): p. 1451-1454.

33. Heller, C., et al., *New 3D-Biophotopolymers with Selective Surface-Cell Interactions for Regenerative Medicine.* Materials Research Society Symposium Proceedings, 2010. **1235**: p. 2-7.

34. Shachaf, Y., M. Gonen-Wadmany, and D. Seliktar, *The biocompatibility of Pluronic®F127 fibrinogen-based hydrogels.* 2010. **31**(10): p. 2836-2847.

35. Lambert, P.M., E.A.C. III, and C.B. Williams. *Design Considerations for Mask Projection Microstereolithography Systems*. in *Solid Freeform Fabrication Symposium*. 2013. Austin, Texas.

36. Jacobs, P.F. *Fundamentals of Stereolithography*. in *Solid Freeform Fabrication Symposium*. 1992.

37. Holzapfel, G.A., *Biomechanics of Soft Tissue*, in *Handbook of Material Behavior Nonlinear Models and Properties*, J. Lemaitre, Editor. 2000, Academic Press: Cachan, France.

38. Annaidh, A.N., et al. *Mechanical Properties of Excised Human Skin*. in *6th World Congress of Biomechanics*. 2010. Singapore.

39. Duprey, A., *Mechanical Properties of the Aorta*, in *Annual Report to the European Society for Vascular Surgery*. 2008.